Thin Film Growth: the Effects of Electronics and Kinetics

Peter Czoschke
Department of Physics
University of Illinois at Urbana-Champaign

Advisor: Prof. Tai-Chang Chiang

In partial fulfillment of the requirements of the Preliminary Examination

May 2, 2003

Abstract

The deposition of thin films is an inherently non-equilibrium thermodynamic process. Thus, kinetics often plays an important role in determining film structure and morphology. Recent growth studies of very thin metal films indicate that confinement of conduction electrons can also alter the behavior of the system such that metastable states of columnar islands of preferred height form. Two experiments are proposed to explore both the structural effects due to quantum confinement and the kinetics governing this interesting system. Both systems will be studied using *in situ* surface x-ray diffraction from a synchrotron source.

I Background

I.a Introduction

Thin films are a ubiquitous component of modern technologies. Despite its widespread use, however, the process of thin film deposition is hardly mundane from a physical perspective. By definition, the growth of thin films is a thermodynamically non-equilibrium process, which means that the same system may exhibit drastically different growth behavior given different deposition conditions (e.g., layer-by-layer growth at low deposition rates versus the formation of three-dimensional islands at high deposition rates) [1].

Hence, thin film growth is often described in terms of kinetics, where growth and evolution of the film are explained in terms of atomistic diffusion and adsorption processes. Local potential barriers and surface energies, such as the energy to form a kink in a ledge, or to diffuse an atom over a terrace edge (the terrace-step-kink model [2, 3]), are used to describe the growth process. However, under certain conditions, collective processes are more important than kinetics of individual atoms and the global energy landscape is the determining factor for the surface morphology and evolution [4]. Two different experiments are proposed to investigate these competing aspects of thin film growth. Both are studies of quantum size effects in ultrathin metal films grown by molecular beam epitaxy (MBE) on semiconductors, where it has been shown that the global energy landscape, which is largely affected by electronic effects, is an important factor determining film morphology [5]. The first experiment explores structural effects of quantum confinement. The second is a temperature dependent film growth study.

I.b Quantum Size Effects in Ultrathin Metal Films

There are three broad categories of thin film growth that encompass the vast majority of observed growth behavior: layer-by-layer (Frank van der Merwe), 3-D island formation (Vollmer-Weber), or a combination of the two in which islands form after one or more initial wetting layers (Stranski-Krastanov) [1]. However, it was recently found that several systems, including Ag/GaAs(110) [6], Ag/Si(111) [7, 8], Pb/Cu(111) [9, 10] and Pb/Si(111) [11, 12, 13] exhibit a peculiar growth behavior where some thicknesses are preferred over others. This effect often manifests itself in the formation of flat-topped, steep-sided islands of the preferred height for a relatively wide range of coverages. The underlying mechanism driving the self-organization of these systems into such structures has been attributed to quantum size effects (QSE), where the minimization of the electronic energy prefers certain thicknesses over others due to quantum confinement of the conduction electrons in the film [14]. These structures are clearly metastable, however, since they require a specific kinetic pathway to form and generally disintegrate after being annealed to sufficiently high temperature [15]. In addition, at different temperatures, different layer thicknesses are preferred. Thus, both thermodynamics and kinetic barriers are important factors in these systems.

Another consequence of QSE that we expect to observe is structural relaxations in the direction of confinement. Previous studies [10, 16] have provided evidence of such layer relaxations related to QSE; however, in most cases, strictly surface probes such at scanning tunneling microscopy (STM) and helium atom scattering (HAS) have been used to deduce step heights. As discussed in Refs. [10, 17], the electron density in these films spills out past the vacuum/film interface, complicating measurements of true layer thicknesses. In contrast, x-rays have a penetration length much longer than the thickness of the films under study and scatter primarily off of the electron density near the ionic cores (for heavier elements, anyway), giving structural information on all the layers in the film.

II Methods and Formalism

II.a Surface X-ray Diffraction (SXRD)

The formalism for surface x-ray diffraction (SXRD) is essentially the same as for traditional x-ray diffraction [18], with the exception that the diffracted intensity must be calculated for a (quasi)-two-dimensional system. The basic idea [19, 20] is that x-rays scatter from electrons, so the amplitude scattered from a small volume element of the system will be proportional to the charge density and have a specific phase. The amplitude of an observed scattered wave with wave vector $\mathbf{k}_f$ (I will only discuss elastic scattering here, so $|\mathbf{k}_f| = |\mathbf{k}_i|$) is then just the coherent sum of amplitudes from each individual volume element. In the case of a crystal, the integral can be easily broken up into the so-called lattice sum

$$A(\mathbf{q}) \propto F(\mathbf{q}) \sum_{j}^{\text{unit cells}} e^{i\,\mathbf{q}\cdot\mathbf{R}_j} \tag{1}$$

where $\mathbf{R}_j$ is a vector in real space to a reference point of unit cell j, $\mathbf{q} = \mathbf{k}_f - \mathbf{k}_i$ is called the momentum transfer, $e^{i\,\mathbf{q}\cdot\mathbf{R}_j}$ is the mentioned phase factor and $F(\mathbf{q})$ is the structure factor for a single unit cell,

$$F(\mathbf{q}) = \int_{\text{unit cell}} \rho(\mathbf{r}) e^{i\,\mathbf{q}\cdot\mathbf{r}} d\mathbf{r} \tag{2}$$

where $\mathbf{r}$ is relative to the unit cell reference point to which the $\mathbf{R}_j$'s point. When doing diffraction from surfaces, it is convenient to work in a surface-based coordinate system such that one basis vector of the crystal (usually $\mathbf{a}_3$) is along the surface normal (the z-direction) and the other two basis vectors ($\mathbf{a}_1$ and $\mathbf{a}_2$) lie in the plane of the surface. If we then make the simplifying assumption that the crystal is a parallelopipedon with N_1, N_2, N_3 unit cells in each respective direction, Eq. (1) becomes

$$A(\mathbf{q}) \propto F(\mathbf{q})\, S_{N_1}(\mathbf{q}\cdot\mathbf{a}_1) S_{N_2}(\mathbf{q}\cdot\mathbf{a}_2) S_{N_3}(\mathbf{q}\cdot\mathbf{a}_3) \tag{3}$$

where $S_N(x)$ is the geometric sum

$$S_N(x) = \sum_{n=0}^{N-1} e^{ixn} = \frac{1-e^{ixN}}{1-e^{ix}}. \tag{4}$$

Since the measured intensity is proportional to $|A|^2$, the quantity of interest is

$$|S_N(x)|^2 = \frac{\sin^2(Nx/2)}{\sin^2(x/2)}. \tag{5}$$

This last equation is called the N-slit interference function and is shown in Fig. 1.

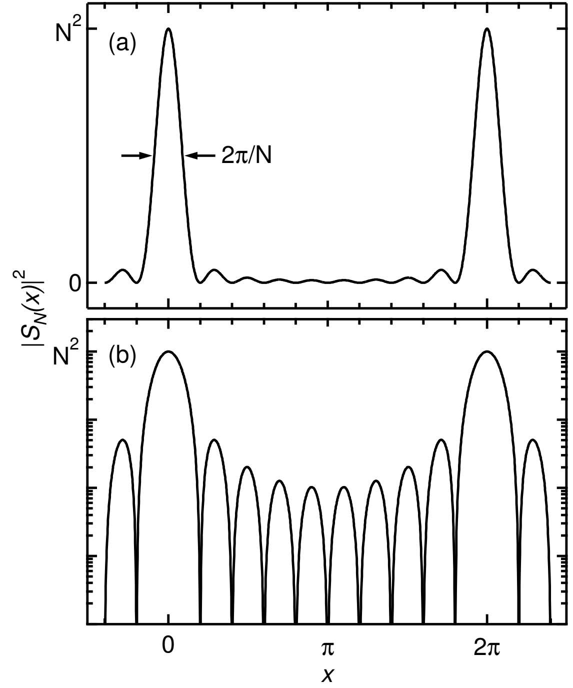

Figure 1: The N-slit interference function for $N = 10$ on (a) a linear scale and (b) a log scale. The height of the main peaks scale as N^2 and become Dirac delta functions in the limit $N \to \infty$. There are $N-2$ maxima in between the two primary peaks, providing for an easy way to determine the number of layers in an ultrathin film.

As can be seen from Fig. 1a, in the limit $N \to \infty$, $|S_N(x)|^2$ becomes a series of Dirac delta functions centered at the points $x = 2\pi n$. In the case of a three dimensional crystal, $N_1, N_2, N_3 \to \infty$ and Eq. (3) describes a lattice of delta functions at the points satisfied by the conditions

$$\mathbf{q}\cdot\mathbf{a}_1 = 2\pi h \tag{6a}$$

$$\mathbf{q}\cdot\mathbf{a}_2 = 2\pi k \tag{6b}$$

$$\mathbf{q}\cdot\mathbf{a}_3 = 2\pi l \tag{6c}$$

where h, k, l are integers. This lattice is the well-known reciprocal lattice. However, for a film-like structure, only $N_1, N_2 \to \infty$ and condition (6c) is relaxed. So the points defined by conditions (6a) and (6b) become smeared out in the $\mathbf{a}_3$ direction, each with a profile like that of Fig. 1. These features are called crystal truncation rods (CTRs) [21]. The curves in Fig. 1 are very regular and symmetric, but that is only due to the ideal nature of the film in the calculation. As will be seen, an actual measured CTR generally has a much richer structure to it that yields a wealth of information about the structure of the film and/or interface.

Notice that there is always a "rod" at $h = k = 0$ which is insensitive to the in-plane structure of the surface. This is the specular, or reflectivity rod, and it offers a useful probe of the structural features normal to the surface; e.g., vertical layer relaxations (which will be discussed in Section III.a). In this case, Eq. (1) becomes

$$A_{film}(q_z) \propto F_{film}(q_z) \sum_{j=1}^{N} e^{i\,q_z z_j} \tag{7}$$

where N now refers to the number of layers in the film, z_j are the positions of the atomic layers in the film, and F_{film} is the structure factor appropriate for the film material. Of course, a film generally sits

atop a substrate which will also contribute its own amplitude of a form similar to Eq. (7) to the scattering for the specular condition. This amplitude must be added coherently to A_{film} before it is squared for the intensity. In practice, the amplitudes of both the film and substrate must be corrected to account for thermal vibrations (Debye-Waller factors, which are material-dependent) and the overall intensity will have experimental corrections that include a factor for the polarization (if any) of the incoming x-rays and a number of geometric factors specific to the type of diffractometer used and how the experiment was conducted [21, 22, 23, 24], all of which are functions of the diffractometer's angular settings and thus indirectly dependent on q_z. The measured scattering intensity will then be

$$I(q_z) \propto (\text{corrections}) \left| A_{sub}(q_z) e^{-M_{sub}} + A_{film}(q_z) e^{-M_{film}} \right|^2 . \tag{8}$$

The M parameters are the Debye-Waller factors.

Experimentally, CTRs are never perfectly sharp in the in-plane directions. That is, conditions (6a) and (6b) never provide for perfect delta functions. Sample mosaicity, finite correlation lengths, and experimental resolution limits are all factors that contribute to finite width of the rods [20]. What is usually measured in the lab is the "integrated intensity", which is the intensity of the rod integrated over a small volume of reciprocal space [18]. The main effect this has on the above results is to add another geometric correction factor to Eq. (8) called the Lorentz factor; however, obtaining the integrated intensity experimentally deserves some mention. The most accurate method for obtaining an integrated intensity of the specular rod is to fix the detector at the appropriate position for the momentum transfer (q_z) desired and then rock the sample about the specular condition. In this manner, a cross-section of the rod is obtained from which the background can be identified and the curve numerically integrated. If the rod is sufficiently narrow, another method which is less time-consuming to do is a "ridge scan". First, the exact alignment of the rod in reciprocal space is determined, the detector slits are then opened up such that the intensity across the whole rod is obtained, and then a scan straight through reciprocal space is done, riding on top of the "ridge" of the specular rod. The background must then be measured by offsetting the detector from the specular condition and repeating the scan. By widening the detector slits, the intensity of a full cross-section of the specular rod is thus measured at once. This method does not integrate over a cross-section perpendicular to the rod in reciprocal space, however, so it introduces additional resolution limitations, but it requires much less time than the rocking curve method.

II.b Quantum Confinement and Quantum Size Effects

If an ultrathin film of metal is adsorbed to a substrate, a first-order approximation for the electronic charge density in the film can be obtained by considering the states in the metal film to be those of a three-dimensional free-electron gas confined in one dimension. The model for such a system would be constructed

as follows. The free-electron wavefunction, $\Psi_{\mathbf{k}}(\mathbf{r}) = \frac{1}{\sqrt{V}} e^{i\mathbf{k}\cdot\mathbf{r}}$, is subjected to the boundary conditions

$$\Psi \rightarrow 0 \qquad \text{at} \qquad z = 0, D. \tag{9}$$

The modified solution for $\Psi_{\mathbf{k}}$ is

$$\Psi_{\mathbf{k}}(\mathbf{r}) = \sqrt{\tfrac{2}{V}}\, e^{i(k_x x + k_y y)}\, \sin k_z z \tag{10}$$

$$\text{where} \qquad k_z = \frac{\pi n}{D} \quad n = 1, 2, 3, \ldots .$$

The electron density at a point $0 \leq z \leq D$ in the quantum well is then

$$\rho(z) = \frac{2V}{(2\pi)^3} \int_0^{k_F} d^3\mathbf{k}\, |\Psi_{\mathbf{k}}(z)|^2 \sum_n \delta\left(k_z - \tfrac{\pi n}{D}\right) \tag{11}$$

$$= \sum_{n=1}^{n_0} 2\pi \left(k_F^2 - k_z^2\right) \sin^2 k_z z$$

$$= \sum_{n=1}^{n_0} 2\pi \left(k_F^2 - k_z^2\right) \frac{1}{2} \left(1 - \cos 2k_z z\right) \tag{12}$$

where $n_0 = \left[\frac{k_F D}{\pi}\right]$, the highest quantum number for the quantum well inside the Fermi surface. We are really interested in the variations in the charge density from a uniform distribution, which can be represented by the dimensionless quantity

$$\delta\rho(z) \equiv \frac{\rho(z) - \langle \rho(z) \rangle_z}{\langle \rho(z) \rangle_z} \tag{13}$$

$$= -\frac{\sum_{n=1}^{n_0} \left(k_F^2 - k_z^2\right) \cos 2k_z z}{\sum_{n=1}^{n_0} \left(k_F^2 - k_z^2\right)} \tag{14}$$

$$= -\frac{1}{C_D} \sum_{n=1}^{n_0} \left(k_F^2 - \left(\frac{\pi n}{D}\right)^2\right) \cos\left(\frac{2\pi n z}{D}\right) \tag{15}$$

where we have recognized that the denominator does not depend on z and becomes a constant prefactor (for a given D) which is positive definite as long as $n_0 < \infty$. Note that the boundary conditions, Eq. (9), become

$$\delta\rho(0) = \delta\rho(D) = -1. \tag{16}$$

Equation (15) appears rather awkward due to the summation over occupied quantum numbers; however, it can be written quite succinctly (and ultimately in closed form, if one would like) in terms of the geometric sum

$$S_D(x) \equiv \sum_{n=1}^{n_0} \cos nx \tag{17}$$

$$= \frac{1}{2} \sum_{n=1}^{n_0} \left(e^{inx} + e^{-inx}\right) \tag{18}$$

$$= \frac{1}{2} \sin n_0 x\, \cot \frac{x}{2} - \sin^2 \frac{n_0 x}{2} \tag{19}$$

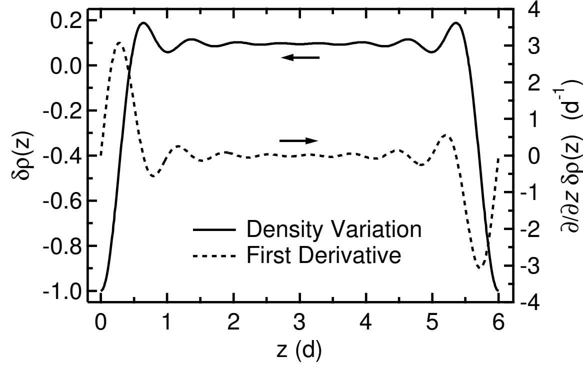

Figure 2: Electron density variation function and its first derivative, Eqs. (21) and (23) (with $A = 1d^2$), for a film with six atomic layers and $k_F = 1.575$ Å^{-1}. The expected positions of the ionic cores would be at the half-integer values on the abscissa.

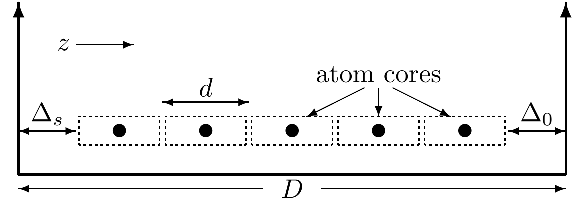

Figure 3: Geometry of the quantum well. The free parameters Δ_s and Δ_0 allow for extra charge spillage at the substrate and vacuum interfaces, respectively.

where the subscript has been added to remind us that S_D, like C_D, implicitly depends on the well thickness D through n_0. Note that

$$\frac{\partial^2}{\partial x^2} S_D(x) = -\sum_{n=1}^{n_0} n^2 \cos nx, \tag{20}$$

which when combined with Eq. (15), leads to the result

$$\delta\rho(z) = -\frac{1}{C_D}\left(k_F^2 + \frac{1}{4}\frac{\partial^2}{\partial z^2}\right) S_D(2\pi z/D). \tag{21}$$

An example of such a density profile for a lead film of $N = 6$ layers can be seen in Fig. 2. The characteristic oscillations evident in Fig. 2 are analogous to the charge density oscillations, commonly referred to as Friedel oscillations, that occur near to the surface of a metal due to the abrupt truncation of the bulk solid [1]. Similar to Friedel oscillations, the oscillations in Fig. 2 have a wavelength approximately equal to π/k_F.

In a real physical system the boundaries of the quantum well are not known *a priori* and for a supported thin film in particular, the two different interfaces will not provide equal levels of confinement. This complication can be addressed by simply defining the well width to be

$$D = \Delta_s + Nd + \Delta_0 \tag{22}$$

where d is the average layer thickness in the film, N is the number of atomic layers and Δ_s and Δ_0 are parameters that account for charge "spillage" past the substrate/film and vacuum/film interfaces, respectively (see Fig. 3). Thus, if no structural relaxations were present, we would expect to find the first layer (next to the substrate) of ionic cores centered at the point $z = \Delta_s + \frac{d}{2}$ in the quantum well.

If these charge oscillations have a structural effect on the atomic positions in the film, we expect it

to be approximately proportional to the first derivative of $\delta\rho$

$$\Delta s(z) = -\frac{A}{C_D}\left(k_F^2\frac{\partial}{\partial z} + \frac{1}{4}\frac{\partial^3}{\partial z^3}\right) S_D(2\pi z/D) \tag{23}$$

where a response coefficient, $A > 0$, has been included. However, these values only have meaning if we choose an arbitrary point of reference. Since the boundary of the quantum well is not necessarily constrained to any absolute relationship with the substrate, choosing such a reference point is problematic. In practice, a less ambiguous quantity to calculate is the thickness of each layer in the film, defined as the distance between atomic planes parallel to the surface. The change in thickness of a layer defined by the atomic planes whose expected positions are z and $z + d$ is therefore

$$\Delta t(z) = -\frac{A}{C_D}\left(k_F^2\frac{\partial}{\partial z} + \frac{1}{4}\frac{\partial^3}{\partial z^3}\right)\left[S_D\left(\frac{2\pi(z+d)}{D}\right) - S_D\left(\frac{2\pi z}{D}\right)\right]. \tag{24}$$

Note that this equation is only valid for $0 < z < D - d$. The actual layer thickness parameters are then obtained by evaluating Eq. (24) at the discrete positions

$$z_j = \Delta_s + j\,d \qquad j = 1, 2, \ldots, N-1; \tag{25}$$

i.e., $\Delta t(z_j)$ is the change in thickness of the layer defined by atomic planes j and $j+1$. The model therefore has four adjustable parameters: A, Δ_s, Δ_0 and d. The last parameter should be very close to the interlayer spacing found in the bulk film material, d_{bulk}, so it is generally more interesting to consider the value of $\delta d \equiv (d - d_{\text{bulk}})/d_{\text{bulk}}$ instead of d.

The chief advantage of such a simple model is that it can be easily and quickly calculated numerically using expressions such as Eq. (20). This makes it possible to incorporate it into a least-squares fitting routine to explain experimental data. This will be done in Section III.a for reflectivity profiles from thin Pb films on Si(111).

III Experiments

III.a Interlayer Relaxations in Pb/Si(111)

As mentioned in Section I.b, systems for which quantum size effects are evident have been posited to have corresponding thickness-dependent layer relaxations. The goal of this first experiment is to look for these layer relaxations and to try to explain them in terms of electronic effects due to QSE. Different preferred island thicknesses have been observed for Pb/Si(111), depending on the interface on which the film is deposited and the temperature at which the film is grown [11]. For this study, films have been grown on two different interfaces: the clean Si(111)-7×7 interface and the commensurate Pb/Si(111)-$\sqrt{3} \times \sqrt{3}$-β interface. Measurements were made using 19.9 keV x-rays from an undulator source at Sector 33, UNICAT

(University-National Laboratory-Industry Collaborative Access Team), Advanced Photon Source, Argonne National Laboratory. Samples were cut from a polished commercial P-doped wafer, degreased and then mounted in an ultrahigh vacuum chamber that is integrated with a z-axis type diffractometer [25]. The sample was mounted to a sapphire block (for electrical isolation) that was thermally anchored to an open-cycle liquid nitrogen refrigerator cold finger. The sample temperature was measured via a thermocouple attached to tantalum clips holding the substrate to the sample mount. In vacuum, the oxide layer covering the Si surface was removed by "flashing" at $\sim 1250°$C for several seconds, after which a sharp 7×7 diffraction pattern was observed with reflection high-energy electron diffraction (RHEED) indicating a clean well-ordered surface. In the case of the $\sqrt{3}\times\sqrt{3}$ samples, 5 Å Pb was then deposited at room temperature and annealed to $\sim$ 415°C until the β-phase was obtained. The surface was confirmed to be in the commensurate β-phase by examining the positions of the diffracted x-ray in-plane superstructure peaks [26]. Pb deposition was accomplished using an *in situ* effusion cell and the rate calibrated using a quartz crystal thickness monitor.

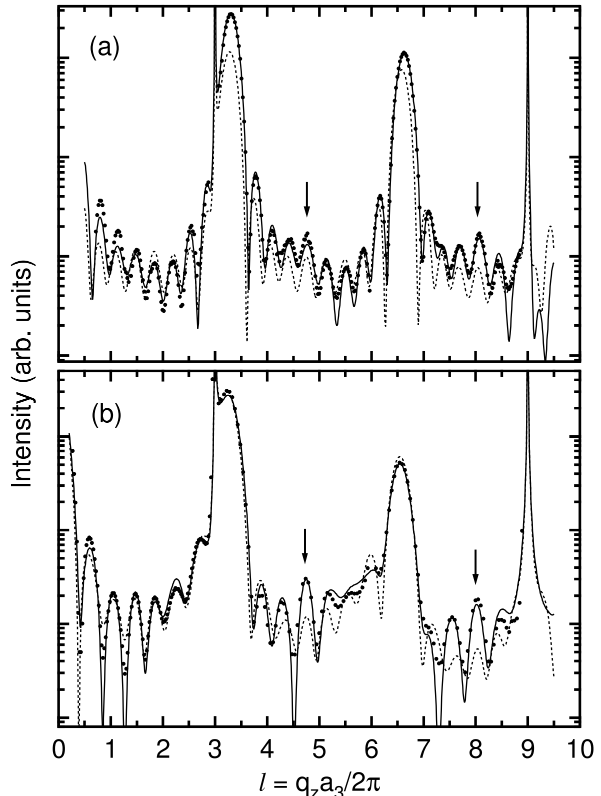

Figure 4: Reflectivity profiles for (a) 8.5 ML Pb deposited on the Si(111)-7×7 interface at 185K and (b) 4.5 ML Pb deposited onto the Pb/Si(111)-$\sqrt{3} \times \sqrt{3}$-β interface at 115K and annealed to 180K. The sharp peaks at $l = 3$ and $l = 9$ are from the bulk Si substrate and the fringes in between from the Pb overlayers. Statistical errors for the experimental data are on the order of the dot size and the solid curves are fits to the model described in the text. For comparison purposes, dashed curves are shown which are fits without any layer relaxations. Arrows point out significant features that are not fit without taking interlayer relaxations into account.

Reflectivity profiles were measured for many different thicknesses and deposition temperatures using a scintillation detector whose angular acceptance was defined via a pair of slits positioned 600 mm from the center of rotation of the diffractometer (to which the sample is oriented). Typical slit settings are 1 mm × 4 mm in and out of the scattering plane respectively, corresponding to a nominal resolution of 0.017 Å^{-1} in q_z at 19.9 keV. Two examples of these profiles are presented in Fig. 4. When describing reflectivity rods, the momentum transfer in the direction of the sample normal will be quoted via the dimensionless variable $l = q_z a_3/2\pi$, where $a_3 = 9.41$ Å is the length

of the Si unit cell in the [111] direction. This is the continuous version of the l in Eq. (6c) for the surface coordinate system. Thus, the bulk-indexed Si Bragg peaks (111) and (333) correspond to $l = 3$ and $l = 9$ respectively. Figure 4a is a reflectivity scan for a sample prepared by depositing 8.5 monolayers (ML) Pb on a freshly prepared Si(111)-7×7 substrate held at 185 K. Here, monolayer coverages are quoted in terms of the bulk surface atom density of Pb(111), 9.43×10^{-14} atoms/cm^2. Measurements were taken with the "rocking curve" method described on page 4. Figure 4b is for a sample with 4.5 ML Pb deposited at 115 K onto the Pb/Si(111)-$\sqrt{3} \times \sqrt{3}$-β interface and then annealed to 180 K. The primary features of the profiles are the two sharp Si Bragg peaks at $l = 3$ and 9, and a complicated pattern of interference fringes from the Pb overlayers. The latter are analogous to the features shown in Fig. 1 where the two larger peaks at $x = 0$ and 2π correspond to the large bumps at $l = 3.3$ and 6.6 in Fig. 4, respectively. The fringes in Figs. 4a and 4b thus indicate that islands of predominantly eight and ten atomic layers (wetting layer included), respectively, are present on the two samples. However, as pointed out in Section II.a, the fringes in Fig. 1 are very regular and symmetric, which is clearly not the case for the experimental curves. In particular, in each case there is a feature roughly halfway between the main Pb peaks that is more pronounced than the neighboring fringes (marked with arrows), which is indicative of some sort of bilayer order in the film; e.g., a bilayer periodicity to the layer relaxations. This phenomenon was reportedly observed in an STM study of the same system [16] and will be discussed further below.

The analytical tools developed in Section II can be used in a least-squares fitting routine to extract structural information from the experimental data. As mentioned in Section II.a, the profile of the reflectivity rod is only sensitive to structural order in the direction of the surface normal ($\mathbf{q} \cdot \mathbf{a}_1 = \mathbf{q} \cdot \mathbf{a}_2 = 0$), so we only need to examine the z-positions of the atomic planes parallel to the surface. Silicon has a diamond lattice structure, so along the [111] direction, the unit cell consists of six lattice planes of alternating spacings of $\frac{1}{4}$ and $\frac{1}{12}$ the length of the unit cell. From Eq. (2), the structure factor for the unit cell is thus (the reference point is the top atom in the unit cell)

$$F_{sub}(l) = f_{\mathrm{Si}}(l) \left(1 + e^{-2\pi i\, l/12}\right) \left(1 + e^{-2\pi i\, l/3} + e^{-4\pi i\, l/3}\right) \tag{26}$$

where the quantity $f_{Si}(l)$ is called the atomic scattering factor and corresponds to Eq. (2) for a single Si atom. Its values are tabulated for different values of $|\mathbf{q}|$ [27]. The substrate scattering amplitude (Eq. (7) for the substrate) for a semi-infinite crystal extending in the $-z$ direction is

$$\begin{aligned} A_{sub}(l) &\propto F_{sub}(l) \sum_{n=0}^{\infty} e^{-2\pi i\, n\, l} \\ &= f_{Si}(l) \frac{1 + e^{-2\pi i\, l/12}}{1 - e^{-2\pi i\, l/3}}. \end{aligned} \tag{27}$$

For the samples grown on the Si(111)-7×7 interface, an additional two underoccupied layers were added to Eq. (27) to account for the surface reconstruction (without the adatom layer) [28].

Since different thickness islands will have different relaxation profiles, the scattering amplitude for the film is

$$A_{film}(l) \propto f_{\text{Pb}}(l) \sum_{\{N\}} \theta_N \sum_{j=1}^{N} e^{2\pi i\, l z_{j,N}}, \qquad (28)$$

where the first sum is over all island thicknesses, θ_N is the fractional coverage of the surface for islands of N atomic layers, and $z_{j,N}$ is the spatial position in units of a_3 for the jth layer of atoms in islands of height N layers. In the fits described below, the $z_{j,N}$ values were calculated via Eqs. (24) and (25). Note that all z values with $j = 1$ are determined by their position relative to the substrate, which was not addressed in the model of Section II.b. They were fit to a shared free parameter z_1.

The solid curves in Fig. 4 are fits using Eqs. (8), (27) and (28) in conjunction with the results from the model presented in Section II.b. Figure 4a was fit with islands of thicknesses between 8 and 12 atomic layers and Fig. 4b was fit using islands of thicknesses between 6 and 12 atomic layers. The results from these fits are summarized in Table I and Fig. 5. Errors were estimated as the range of parameter values that doubled the χ^2 value of the fit. The quality of the fits in Fig. 4 are a good indication that the structural features of the system have been adequately described by the model. Careful examination of the data points in Figs. 5a and 5b shows that the layer thicknesses $\Delta t(z_j)$ roughly follow a bilayer alternation that is damped with film penetration. As mentioned on page 9, this bilayer relaxation phenomenon has been suggested by STM studies but remains unconfirmed. The parameters in Table I are difficult to interpret without correlations from further datasets. It would be interesting, for instance, to see if there are thickness dependent oscillations in the Δ_0 and Δ_s parameters as predicted in Ref. [10] and as seen as fringes in STM images of quantum wedges [29]. Finally, the response coefficient A may give an indication of the magnitude of out-of-plane strains produced by QSE.

Table I: Parameters for the model described in Section II.b for the fits in Fig. 4. Future correlation of these values with other datasets could provide insights into the nature of the structural effects of QSE.

Parameter	7×7 N=10	$\sqrt{3} \times \sqrt{3}$-β N=8
A (Å^2)	86±35	135±35
Δ_s (Å)	0.36±0.05	0.76±0.25
Δ_0 (Å)	0.9±0.4	0.31±0.08
δd (%)	-0.90±0.31	-0.77±0.65

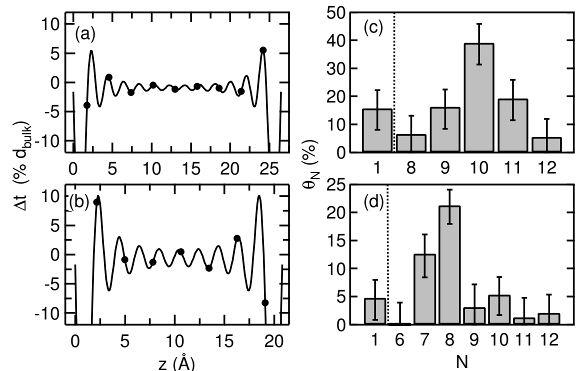

Figure 5: Results for the fits in Fig. 4. Values for Δt and continuous curves using Eq. (24) and the parameters in Table I are shown in (a) for the N=10, 7×7 sample in Fig. 4 and (b) for the N=8, $\sqrt{3}\times\sqrt{3}$ sample. Points are actual thickness values, $\Delta t(z_j)$. The occupancy values from the fits, θ_N are shown in (c) and (d) for the two samples, respectively. Values are in percentage surface area covered assuming bulk Pb surface atom density.

III.b Island Growth in Pb/Si(111)

Films of Pb on Si(111) deposited at room temperature form 3-D structures following the Stranski-Krastanov growth mode. It is only at low temperatures that you either observe layer-by-layer growth or the formation of flat-topped islands of preferred thicknesses as mentioned in Section I.b. However, if the film is deposited at low temperature and then annealed, one finds that islands irreversibly change to a new preferred height. That is, different preferred heights are observed for different kinetic pathways. Hence, both thermodynamics and kinetics appear to be intimately involved in the selection of the preferred height for a given temperature, neither of which are fully understood at present. The study of this height selection could potentially yield interesting insights into kinetic barriers and variables and their relationship to QSE.

Previous STM and HAS studies of the Pb/Si(111) system have suggested that the preferred thicknesses for different temperatures differ in bilayer increments [17, 30]. If true, we expect to see growth of island height in bilayer steps as the sample is annealed. The following is a proof of principle in the use of SXRD to study this phenomenon. In Section II.a it was already mentioned that the number of fringes in Fig. 1 indicated the number of layers in the film. Here, this property will be extended to show how different growth behaviors manifest themselves in reflectivity profiles.

Figure 6 shows evolving reflectivity profiles for two different types of growth behavior. For the sake of clarity, the calculations were done for a mock film with no contribution from the substrate. This was done because the features discussed below are more obvious without the substrate contribution and remain qualitatively the same. Calculations were done by constructing an amplitude similar to Eq. (7) with $F_{film}(q_z) = 1$ and allowing for multiple film thicknesses, which are added together coherently. Assuming that all layers have uniform spacing a_3,

$$A(q_z) = \sum_{\{N\}} \theta_N S_N(q_z a_3) \tag{29}$$

where the sum is over all thicknesses and θ_N is the fractional coverage of the surface for thickness N. That is, $\sum_{\{N\}} \theta_N = 1$ and the total coverage of the film in monolayers is

$$\Theta = \sum_{\{N\}} N\theta_N. \tag{30}$$

Equation (29) corresponds to a film that is flat on one side (which would be the film/substrate interface) and stepped on the other.

Figures 6a and 6b show reflectivity profiles for layer-by-layer growth in the range 5-8 ML in $\frac{1}{5}$ ML increments. Figures 6c and 6d show profiles for bilayer growth in the range 5-10 ML in $\frac{1}{3}$ ML increments. Each type of growth mode is shown with two different degrees of roughness to illustrate its qualitative effect. The abscissae are the same as in Fig. 1; i.e., the larger bumps at $x = 0$ and 2π are where Bragg peaks would

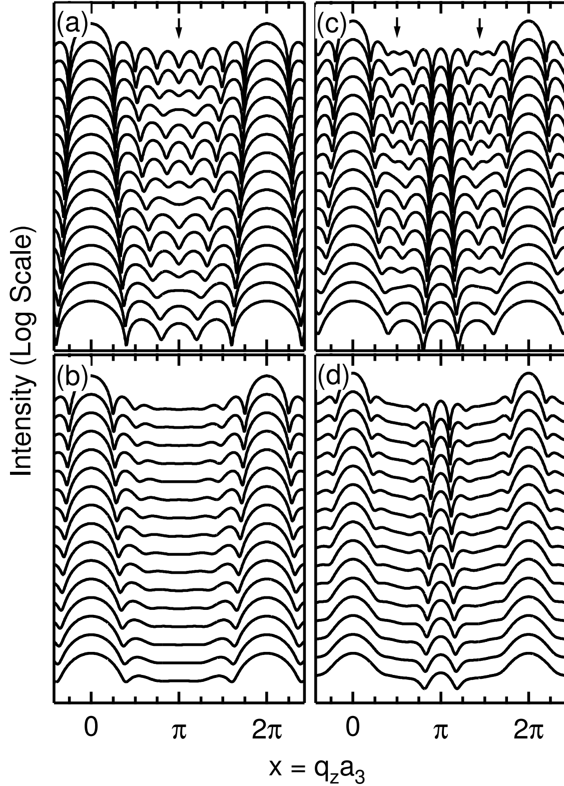

Figure 6: Illustration of different film morphologies during growth. (a) Layer-by-layer growth with minimal interface roughness and (b) moderate interface roughness for Θ=5-8 ML. (c) Bilayer growth (only odd N thicknesses allowed) with minimal roughness and (d) moderate roughness for Θ=5-10 ML. For layer-by-layer growth, new fringes form at the "anti-Bragg" point $x = \pi$, whereas for bilayer growth, new fringes form closer to the points $x = \frac{\pi}{2}, \frac{3\pi}{2}$. Even with moderate roughness, bilayer growth has a distinctive feature at $x = \pi$.

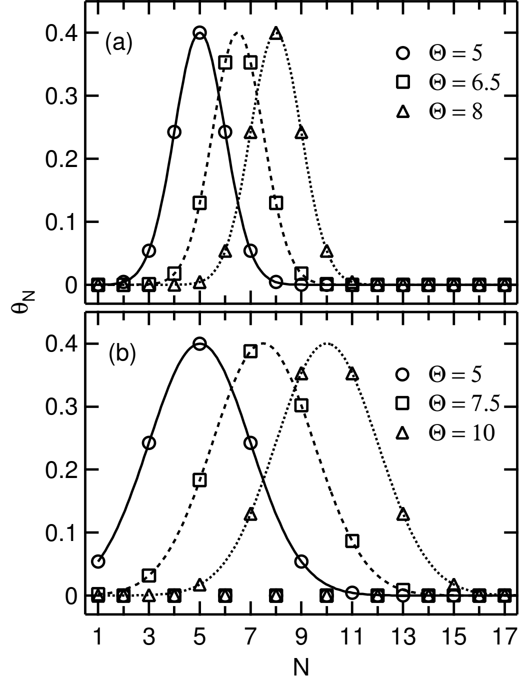

Figure 7: Examples of profiles for the relative occupancy parameters θ_N. Relative coverages for (a) layer-by-layer and (b) bilayer growth as shown in the bottom, middle and top curves of Figs. 6b and 6d ($\sigma = 1$ and $\sigma = 2$, respectively). The coverage profiles for Figs. 6a and 6c are similar but with Gaussian distributions of half the width.

be found as $N \to \infty$. The θ_N follow a Gaussian distribution centered at Θ:

$$\theta_N = \frac{A}{\sigma} \exp\left(-\frac{(N-\Theta)^2}{2\sigma^2}\right) \tag{31}$$

where the constant A is dynamically chosen such that Eq. (30) is satisfied. Bilayer growth was modelled in the same manner but only allowing alternating θ_N to be non-zero (odd N in this case). In the case of Fig. 6, $\sigma = 0.5$, 1, 1 and 2 for (a), (b), (c) and (d) respectively. Examples of the occupancy parameter profiles for selected curves from Figs. 6b and 6d are shown in Fig. 7.

As can be seen, there are distinct qualitative differences that manifest themselves depending on the growth mode. For smooth monolayer growth, all of the interference fringes are well-defined, whereas rougher growth tends to smear out the fringes away from the Bragg positions. As the film grows, the fringes

collectively move away from the so-called "anti-Bragg" position at $x = \pi$, making room for a new fringe indicating the formation of a new layer. In contrast, for bilayer growth layers form in pairs, so there is no contribution from even thicknesses. As the coverage increases, the fringes at the anti-Bragg position remain fixed, letting two new fringes form close to $x \approx \frac{\pi}{2}$ and $\frac{3\pi}{2}$ simultaneously. Even for a moderately rough interface, the bilayer property is clearly distinguishable.

Figure 8 shows experimental reflectivity profiles for a single coverage of 4.5 ML Pb deposited onto the Pb/Si(111)-$\sqrt{3} \times \sqrt{3}$-β interface. The deposition was done at low temperature (113 K), where it is known that the film grows layer-by-layer. Since the $\sqrt{3} \times \sqrt{3}$-β interface has a nominal coverage of 0.28 ML, we expect to see primarily $N = 5$ thicknesses in the reflectivity, which is clearly the case at 113 K. Upon annealing to 153 K, it can be seen that islands six atoms high have formed. At around 168 K, extra space can be seen to form at the positions we'd expect for bilayer growth, ($l \approx 0.75, 2.25, \ldots$, which correspond to the points $x = \frac{\pi}{2}, \frac{3\pi}{2}$ in Fig. 6c). The thickness ($N = 8$) remains stable up to around 183 K, after which it appears to grow by another bilayer and clear signs of roughening appear, but the characteristic fringes at $l \approx 1.6$, 5 and 8 remain (corresponding to the fringes at $x = \pi$ in Figs. 6c and 6d), indicating a clear preference for island thicknesses differing in bilayers (and of even N, incidentally).

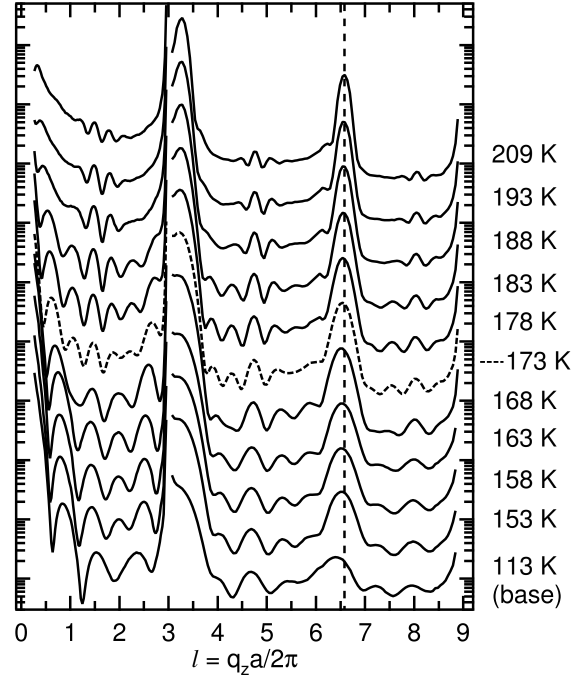

Figure 8: Reflectivity profiles for a sample with 4.5 ML Pb deposited on the $\sqrt{3} \times \sqrt{3}$-β interface at 113 K and then annealed. As more thermal energy is added to the system, islands first grow by a monolayer and then in bilayers. The curve for 173 K is dashed to serve as a guide to the eye.

The presence of distinct interference fringes up until ~ 180 K indicates an initially low degree of roughness at the film/vacuum interface; therefore, the prominent features at the anti-Bragg conditions ($l \approx 4.75$ and 8) for low temperatures seem to be related to the bilayer relaxation phenomenon discussed in Section III.a. However, at higher temperatures where substantial contribution from multiple island heights is apparent, we expect the relaxation effects to be smeared out. In addition, the presence of multiple bumps at the anti-Bragg conditions is very similar to the simulated profiles in Fig. 6 and is thus believed to be due to the bilayer height selection phenomenon instead of interlayer relaxations. Supporting this claim is the movement of the second Pb peak at $l = 6.4$ towards the dashed line at $l = 6.58$ (the position for bulk Pb) as temperature is increased, indicating a gradual change in

average layer spacing towards the bulk expected value. Detailed analysis of the data will definitively answer this question.

IV Summary

This proposal has reviewed some of the interesting and often surprising effects due to quantum confinement in metal on semiconductor systems. It was suggested that surface x-ray diffraction could provide valuable insight into these phenomena that contrasts with the existing body of research. Preliminary results for the Pb/Si(111) system have been presented which show a connection between the electronic charge density and structural properties of the Pb overlayers. This study will be continued with the acquisition of further data on samples grown at different temperatures and/or on different interfaces. In addition, an experiment in which islands of a columnar nature can grow taller through careful annealing were introduced. By studying samples prepared with different initial coverages and/or different annealing temperatures/rates, we can learn about the kinetics involved in the formation of these unusual structures.

References

[1] A. Zangwill. *Physics at Surfaces*. Cambridge University Press, 1988.

[2] John A. Venables. *Introduction to Surface and Thin Film Processes*. Cambridge University Press, 2000.

[3] Zhenyu Zhang and Max G. Lagally. Atomistic processes in the early stages of thin-film growth. *Science*, 276:377, 1997.

[4] Ruud M. Tromp and James B. Hannon. Thermodynamics of nucleation and growth. *Surf. Rev. and Lett.*, 9:1565, 2002.

[5] Hawoong Hong, C.-M. Wei, M. Y. Chou, Z. Wu, L. Basile, H. Chen, M. Holt, and T.-C. Chiang. Alternating layer and island growth of Pb on Si by spontaneous quantum phase separation. *Phys. Rev. Lett.*, 90:076104, 2003.

[6] Arthur R. Smith, Kuo-Jen Chao, Qian Niu, and Chih-Kang Shih. Formation of atomically flat silver films on GaAs with a "silver mean" quasi periodicity. *Science*, 273:226, 1996.

[7] L. Gavioli, K. R. Kimberlin, M. C. Tringides, J. F. Wendelken, and Z. Zhang. Novel growth of Ag islands on Si(111): Plateaus with a singular height. *Phys. Rev. Lett.*, 82:129, 1999.

[8] Lin Huang, S. Jay Chey, and J. H. Weaver. Metastable structures and critical thicknesses: Ag on Si(111)-7×7. *Surf. Sci.*, 416:L1101, 1998.

[9] B. J. Hinch, C. Koziol, J. P. Toennies, and G. Zhang. Single and double layer growth mechanisms induced by quantum size effects in Pb films deposited on Cu(111). *Vacuum*, 42:309, 1991.

[10] Giuliana Materzanini, Peter Saalfrank, and Philip J. D. Lindan. Quantum size effects in metal films: energies and charge densities of Pb(111) grown on Cu(111). *Phys. Rev. B*, 63:235405, 2001.

[11] V. Yeh, L. Berbil-Bautista, C. Z. Wang, K. M. Ho, and M. C. Tringides. Role of the metal/semiconductor interface in quantum size effects: Pb/Si(111). *Phys. Rev. Lett.*, 85:5158, 2000.

[12] M. Hupalo, S. Kremmer, V. Yeh, L. Berbil-Bautista, E. Abram, and M. C. Tringides. Uniform island height selection in the low temperature growth of Pb/Si(111)-(7x7). *Surf. Sci.*, 493:526, 2001.

[13] M. Hupalo, V. Yeh, L. Berbil-Bautista, S. Kremmer, E. Abram, and M. C. Tringides. Uniform height island growth of Pb on Si(111)-Pb($\sqrt{3} \times \sqrt{3}$) at low temperatures. *Phys. Rev. B*, 64:155307, 2001.

[14] Zhenyu Zhang, Qian Niu, and Chih-Kang Shih. "Electronic growth" of metallic overlayers on semiconductor substrates. *Phys. Rev. Lett.*, 80:5381, 1998.

[15] Hongbin Yu, C. S. Jiang, Ph. Ebert, X. D. Wang, J. M. White, Qian Niu, Zhenyu Zhang, and C. K. Shih. Quantitative determination of the metastability of flat Ag overlayers on GaAs(110). *Phys. Rev. Lett.*, 88:016102, 2002.

[16] W. B. Su, S. H. Chang, W. B. Jian, C. S. Chang, L. J. Chen, and Tien T. Tsong. Correlation between quantized electronic states and oscillatory thickness relaxations of 2D Pb islands on Si(111)-(7x7) surfaces. *Phys. Rev. Lett.*, 86:5116, 2001.

[17] Jens Braun and J. Peter Toennies. Observation of a quantum size effect in the surface electron density of thin lead films. *Surf. Sci.*, 384:L858, 1997.

[18] B. E. Warren. *X-ray Diffraction*. Dover Publications, Inc., 1969.

[19] I. K. Robinson and D. J. Tweet. Surface x-ray diffraction. *Rep. Prog. Phys.*, 55:599, 1992.

[20] Jens Als-Nielsen and Des McMorrow. *Elements of Modern X-Ray Physics*. John Wiley and Sons, Ltd., 2001.

[21] I. K. Robinson. Crystal truncation rods and surface roughness. *Phys. Rev. B*, 33:3830, 1986.

[22] R. Feidenhans'l. Surface structure determination by x-ray diffraction. *Surf. Sci. Rep.*, 10:105, 1989.

[23] E. D. Specht and F. J. Walker. A method for the accurate determination of crystal truncation rod intensities by x-ray diffraction. *J. Appl. Cryst.*, 26:166, 1993.

[24] I. K. Robinson. Structure factor determination in surface x-ray diffraction. *Aust. J. Phys.*, 41:359, 1988.

[25] J. Mati Bloch. Angle and index caculations for a 'z-axis' x-ray diffractometer. *J. Appl. Cryst.*, 18:33, 1985.

[26] F. Grey, R. Feidenhans'l, M. Nielsen, and R. L. Johnson. The relationship between the metastable and stable phases of Pb/Si(111). *Colloque de Physique*, C7:181, 1989.

[27] *International Tables for X-ray Crystallography, vol. C*, 1992.

[28] Kunio Takayanagi, Yasumasa Tanishiro, Shigeki Takahashi, and Masaetsu Takahashi. Structure analysis of Si(111)-7×7 reconstructed surface by transmission electron diffraction. *Surf. Sci.*, 164:367, 1988.

[29] I. B. Altfeder, K. A. Matveev, and D. M. Chen. Electron fringes on a quantum wedge. *Phys. Rev. Lett.*, 78:2815, 1997.

[30] M. Hupalo and M. C. Tringides. Correlation between height selection and electronic structure of the uniform height Pb/Si(111) islands. *Phys. Rev. B*, 65:115406, 2002.